STUDY OF THE INFLUENCE OF CONDUCTIVE DEFECT CHARACTERISTICS ON EDDY CURRENT DIFFERENTIAL PROBE SIGNAL

N. BENHADDA[1] T. BOUCHALA[2] A. GUETTAFI[1] and B. ABDELHADI[1]

[1]Electrical Engineering Department, El-Hadj Lakhdar University, Batna. Laboratory of Electric Traction Systems – Batna (LSTE - Batna), Alegria.

[2]Electrical Engineering Department, Kasdi Merbah University, Ouargla, Algeria.

nabil_benhadda@yahoo.fr, bouchala.tarek@univ-ouargla.dz, amor_guettafi@yahoo.fr, abdelhadi3b@yahoo.com

Abstract *– Nowadays, numerical modelling has become an interesting tool for determining impedance variations due to various conductive flaws in eddy current non-destructive evaluation systems. These kinds of defects, rarely treated in the published works, are taken into consideration in the modelling while introducing them as electrically conductive volumes with a finite electric resistivity. This step is very important since it permits to improve qualitatively several models developed so far by many authors whose consider the defect as loss of material only. However, in several applications, the defect can occur with a finite resistivity such as impurity, small burns and micro-solder. On the other hand, even though the defect appears with a loss of materials, some polluting materials can fill the affected region. Indeed, the volume of the initial defect will be completely or partially occupied by these conducting pollutant materials. This paper deals with the effect of physical and geometrical characteristics of such kind of defects on the differential sensor response. Furthermore, the necessity of taking the defect electric conductivity (as an important parameter) into account will be explained, in order to develop a reliable and accurate inverse method allowing a full characterization of conductive defects.*

Keywords: *Eddy Current, Differential Sensor, Conductive Defect.*

1. Introduction

The eddy current technique is one of the preferred Non Destructive Testing (NDT) methods for the inspection of deployed metallic components [1]. It is a fast and effective method of defect detection in metal rods and plates caused by corrosion or stress [2]. Eddy Current Testing (ECT) requires an excitation coil to induce currents within the sample conductive material. In the presence of a defect, these currents are perturbed and thus, the produced magnetic field is also perturbed. Eddy current sensor is used for detecting this perturbed field. These field perturbations are then processed to infer on the defect presence and its physical and geometrical characteristics. Until now, the majority of the published scientific works in the literature treating eddy current testing have elaborated the detection and the characterization of defect existing in the material as a loss of material. However, other defects can appear without loss of material; one can state as examples the small inclusions, small burns and micro-solders, [3].

In fact, even though the defect appears with a loss of materials, some polluting materials can fill and occupy the affected region. Indeed, the volume of the initial defect will be completely or partially occupied by these conducting pollutants materials; that can be the sit of induced currents. Therefore, if this phenomenon is not taken into consideration in the modeling of these systems, the results with this assumption will be affected. In this article, the effect of this parameter on the signature of the defect will be made into evidence. In other words, the effect of physical and geometrical parameters of this kind of defects such as its depth, width and electric conductivity on a differential probe signal will be studied. The advantage of differential coils is being able to detect very small discontinuities and permits to eliminate temperature and lift-off variation effects, [11].

2. Eddy current testing through Maxwell equations

Maxwell's equations describe the physical model used for electromagnetic EC problems solved with the finite element method (FEM) that allows determining the response of sensor eddy current. The magnetic vector potential, electric and magnetic field or the pointing vectors are the most quantities widely used to solve the field equations, [2]. Quasi-stationary Maxwell equations are given hereafter:

$$\nabla \times \vec{H} = \vec{J}_s \tag{1}$$

$$\nabla \times \vec{E} = -\frac{\partial \vec{B}}{\partial t} \tag{2}$$

$$\nabla . \vec{D} = 0 \tag{3}$$

$$\nabla . \vec{B} = 0 \tag{4}$$

The constitutive relations describing the material properties in relation to the electromagnetic fields are given by:

$$\vec{B} = \mu \vec{H} \quad (5)$$

$$\vec{J} = \sigma \vec{E} \quad (6)$$

In equations (1) to (4), H is the magnetic field, E is the electric field, B is the magnetic flux density, D is the electric flux density, J_s is the coil current density, and t is the time. The magnetic potential vector A can be determined through the following equation:

$$\vec{B} = \nabla \times \vec{A} \quad (7)$$

By replacing equation (7) into equation (2) we can write:

$$\vec{E} = -\frac{\partial \vec{A}}{\partial t} \quad (8)$$

Since:

$$\vec{J} = \sigma \vec{E} = -\sigma \frac{\partial \vec{A}}{\partial t} \quad (9)$$

By introducing equation (9) into equation (1), we obtain:

$$\frac{1}{\mu}(\nabla \times \nabla \times \vec{A}) = \vec{J_s} - \sigma \frac{\partial \vec{A}}{\partial t} \quad (10)$$

If ω is the applied angular frequency and by considering $\nabla \vec{A} = 0$ (coulomb gauge), for time-harmonic electromagnetic fields, equation (10) could be expressed as:

$$\frac{1}{\mu} \nabla^2 \vec{A} = -\vec{J}_s + j\omega\sigma \vec{A} \quad (11)$$

3. Axi-symmetrical model

Since the testing model has characteristics of axial symmetry, it could be described by cylindrical coordinate system (r, θ, z), [2].

In the case of axisymmetric geometries, where A and J_s have components at the positive direction of θ only equation (11) could be written as given in, [4-5]:

$$\frac{1}{\mu}\left(\frac{\partial^2 \vec{A}}{\partial r^2} + \frac{1}{r}\frac{\partial \vec{A}}{\partial r} + \frac{\partial^2 \vec{A}}{\partial z^2} - \frac{\vec{A}}{r^2}\right) = -\vec{J}_s + j\omega\sigma \vec{A} \quad (12)$$

Where A is the magnetic vector potential (Wb/m), J_s is the source current density (A/m), μ and σ are the permeability (Wb/Am), and conductivity (S/M), respectively.

Equation (12) is a linear diffusion equation for sinusoidal steady state condition and axisymmetric geometries. For a given situation, the magnetic vector potential can be found by solving the above equation using appropriate boundary conditions, [4]**.** The electromagnetic system is composed of test specimen, sensor coils and air. The equation governing the conductive rod is given as follows.

$$\Delta \vec{A} = \mu \sigma_p \frac{\partial \vec{A}_1}{\partial t} \quad (13)$$

Where σ_p represents the conductivity of specimen

The equation representing sensor coil is given by:

$$\Delta \vec{A} = \vec{J}_s \quad (14)$$

The differential equation for the air-filled space between the tested rod and the coil is Laplace's equation which is given by, [4]:

$$\Delta \vec{A} = 0 \quad (15)$$

The most models studied so far suppose that the defect (flaw) is an air that is integrated in equation (15).

Some studies have published papers related to the conductivity of the test piece, as it is one of the most important variables in eddy current testing. Shao and al. [6], presented a method for the reconstruction of conductivity profiles from eddy current impedance change data but in this article, we suppose that the defect is as a conductive volume which is different from the one governing the test piece as presented in the following equation:

$$\Delta \vec{A} = \mu \sigma_d \frac{\partial \vec{A}}{\partial t} \quad (16)$$

Where σ_d is the defect conductivity.

4. Finite element discretization

For solving equation (12), we have used the finite element (FE) method. An energy functional equivalent to the diffusion equation (Eq. (12)) is formulated based on the energy balance in the solution region. The region is discretized using first-order triangular elements and the energy balance within the entire region W was achieved by minimizing the energy functional at every node in the region as given in [5].

Applying energy minimization, the final element matrix equation is obtained as done in, [7, 8]:

$$W(\mathrm{A}) = \iint_S \left[\frac{1}{2\mu}\left(\left|\frac{\partial A}{\partial z}\right|^2 + \left|\frac{\partial A}{\partial r} + \frac{A}{r}\right|^2\right) + j\sigma\omega|A|^2 \right] r dr dz \quad (17)$$

Where S is the solved region.

The solution now consists of finding a set of functions A such that the energy-related functional is minimized. Since this cannot be done everywhere in space, a bounded region (solution region) is discretized into a large number of linear triangular elements. In each element, three nodal points are defined at which the magnetic vector potential is found. Minimization of the energy functional is achieved by setting the partial derivative with respect to each nodal value A_i equal to zero, **[**5-8**]**:

$$\frac{\partial W(A)}{\partial A_i} = 0, \qquad i = (1, 2, 3) \qquad (18)$$

Where I is the total number of the nodes in the solution region. After rearrangement, we get the linear algebra equations set of nodal vector potential of each element e as given in [9, 10]:

$$\{[K]_e + j[R]_e\}[A]_e = [Q]_e \qquad (19)$$

Equation (19) is called the cell matrix equation of element e. These elements can be combined into an N-order complex gross matrix equation (N is the sum of the nodes):

$$\{[K] + j[R]\}[A] = [Q] \qquad (20)$$

And:

$$[G][A] = [Q] \qquad (21)$$

Where $[G]$ is an $N \times N$ orders symmetric zonal complex coefficient matrix (gross stiffness matrix); $[A]$ is the unknown $N \times 1$ orders nodal complex vector potential and $[Q]$ is the $N \times 1$ orders nodal source complex vectors to be solved, [8].

5. Solving the Finite Element Equations

The Gauss elimination algorithm is applied to the system of equations, taking advantage of the symmetry [7]. Once the magnetic potential is calculated, the other physical quantities, such as magnetic flux, induced EC density, magnetic energy, EC losses and impedance variations, can be calculated for each displacement step of the sensor. The total impedance of a differential probe can be calculated by the following expression, [5].

$$Z_{probe} = \frac{j2\pi\omega N_C}{I^2}\left(\sum_{k=1}^{k1} r_k \Delta_k A_k + \sum_{k=1}^{k2} r_k \Delta_k A\right)_k \qquad (22)$$

Where k_1 and k_2 are the number of elements in the two coils, Nc is the turn density of the coils, I is the current in a turn of the coils, r_k is the distance from the element centroid to the symmetry axis, Δ_k is the area of element on the cross section of the coil and A_k is the A at the centroid.

6. Studied device description

Differential probes consist of two coils that compare two adjacent parts of the inspected material as shown in Fig. (1). The detecting coils are wound in the opposite directions the one to the other in order to equalize the induced voltages generated by the excitation primary field. Differential coils have the advantage of being able to detect very small discontinuities. However, differential coils do no detect gradual dimensional or composition variations of the test piece, as the coils are typically very close, [11]. Fig. (1) presents the studied configuration which is composed of twin coils that generates two conflicting electromagnetic fields. Each coil is made of a copper wire with a conductivity of 59.6MS/m [12], a height of 3 mm and has a coil of 70 turns and a width of 2.6 mm. The inspected piece is a rod with a radius of 4 mm and a length of 60 mm, the lift-off is of 0.1 mm. Knowing that the electrical currents in both coils of the sensor are equal in intensity and opposite in direction, one can write as: $J_T = J_{C1} = -J_{C2}$ since the studied geometry is axis-symmetric, the domain of solution is reduced to half of the device as shown in Fig. (1).

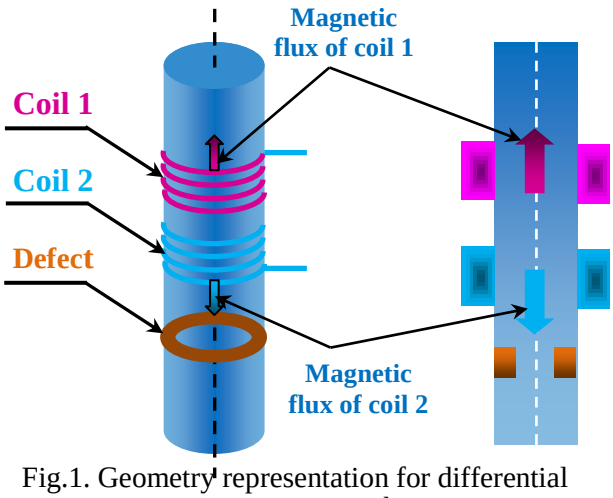

Fig.1. Geometry representation for differential sensor probe.

7. Effect of defect parameters on differential probe impedance

In the following sections, the developed model has been exploited to study the effect of the variation of rectangular cross section defect geometrical and physical parameters on differential sensor impedance. Moreover, for analyzing the effect of excitation field frequency, three frequencies 100, 240 and 500 kHz have been introduced. The defect parameters to be studied are the depth D_d, the width L_d and the electric conductivity σ_d.

7.1. Effect of defect depth D_d

The fulfillment of this study requires the variation of the defect depth for the three frequencies while maintaining its width fixed at 1mm. The sensor impedance is calculated for different positions, from -20mm to 20mm, according to the z axis as illustrated in Fig. (2). When the sensor does not detect any defect, the variations of the impedance components (absolute of Z and lissajou) are null. When the sensor is coming near the defect, we observe an increase in the variation of these components up to a maximal value. This increase is due to the fact that the first coil of the sensor sees the defect in a position different from the one of the second coil. This induces a variation of the field and consequently a variation in the impedance. When the sensor arrives in front of the defect, no variation is recorded since the two coils are symmetrically located at the same position compared to the center of the defect, [11].

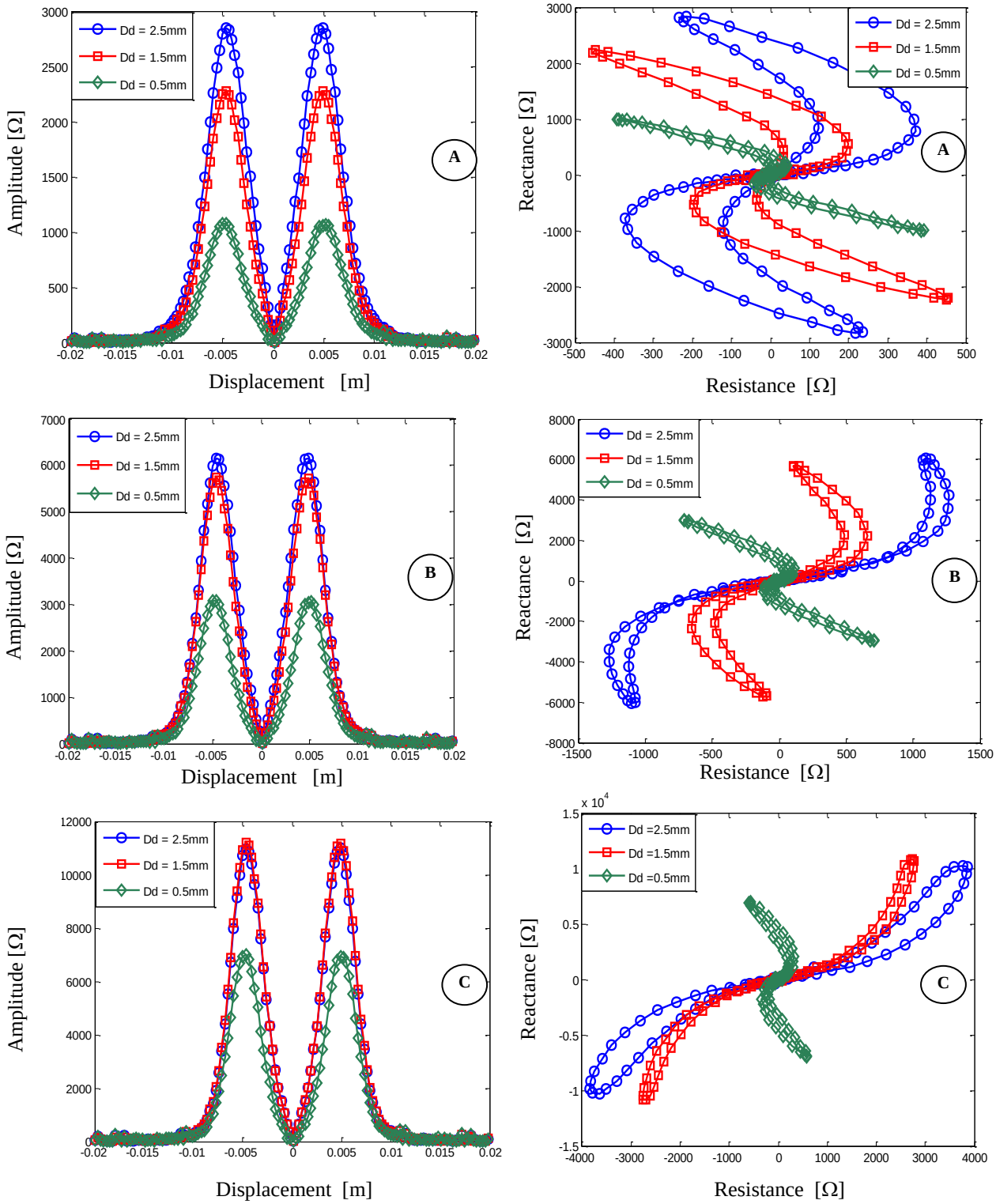

Fig. 2 Evolution of sensor impedance parameters according to width variation.
(A): f=100kHz, (B): f=240kHz, (C): f=500kHz,

We notice that when the defect depth increases the amplitude of the signal increases too. Similarly, the signal amplitude increases when the frequency increases. Furthermore, according to the Lissajou curves, the differential impedance phase varies clockwise with the increase of defect depth.

7.2. Effect of defect width

The accomplishment of this study necessitates the variation of the defect width for the three frequencies while maintaining its depth fixed at 2mm. The sensor impedance is calculated for different positions, from -20mm to 20mm, according to the z axis as illustrated in Fig. (3).

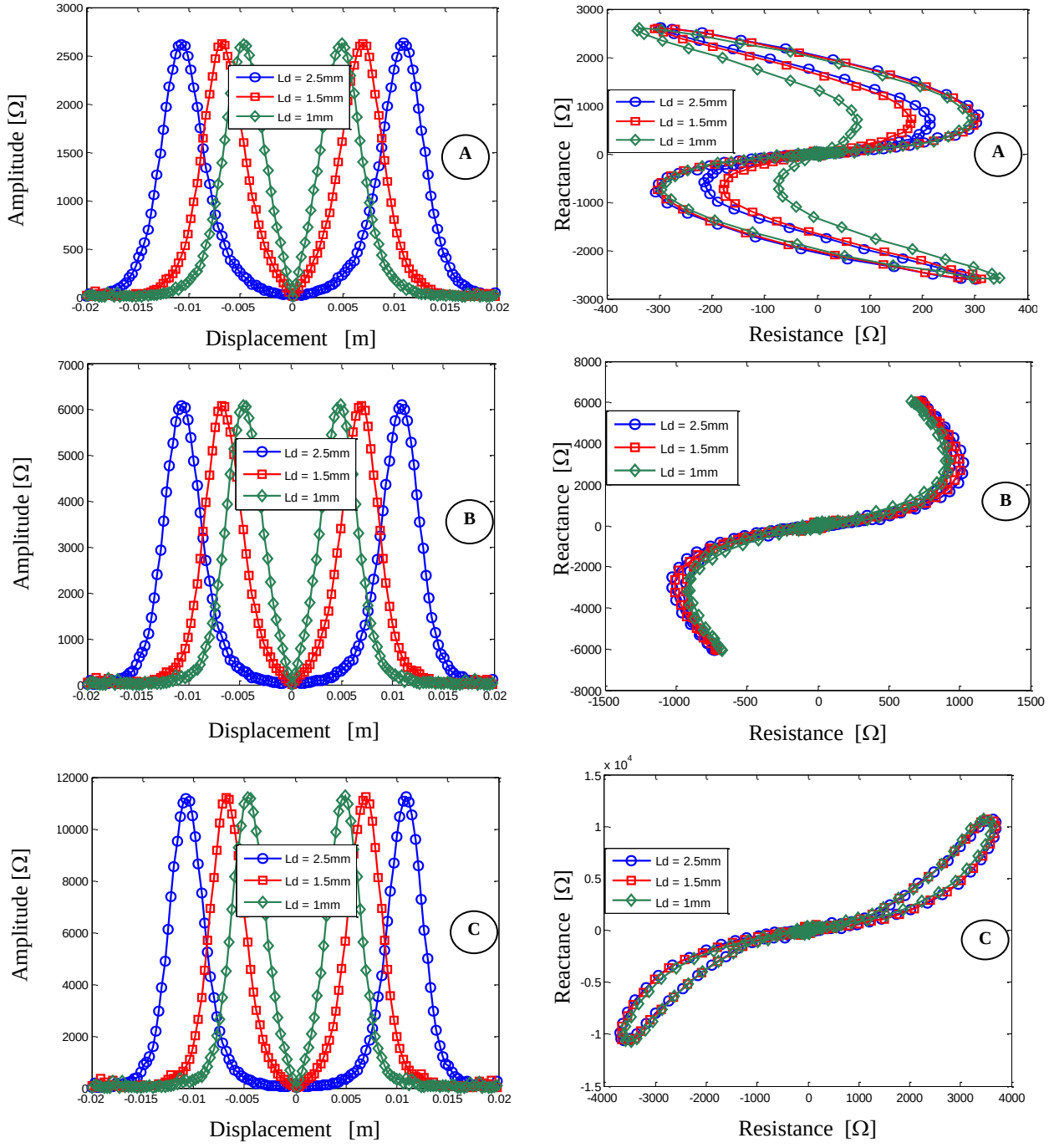

Fig. 3 Evolution of sensor impedance parameters according to defect width (L_d).
(A): f=100kHz, (B): f=240kHz, (C): f=500kHz,

According to the curves depicted in Fig. (3), we notice that the amplitudes and the phases of the signal remain nearly unchanged for all widths whereas the distance between the two peaks of impedance increases when the defect width increases. Furthermore, the amplitude of the signal becomes more important when the frequency increases.

7.3. Effect of defect electric conductivity

The purpose of the following simulations is to study the influence of defect electric conductivity on the differential probe impedance variation, since its omission would lead to incomplete and affected results. Generally, several factors can affect locally the electric conductivity such as presence of impurities, small burns and micro-solder, [3]. In this case, the defect differ by its electric conductivity variation while maintaining constant the other parameters (D_d=2mm and L_d=1mm).

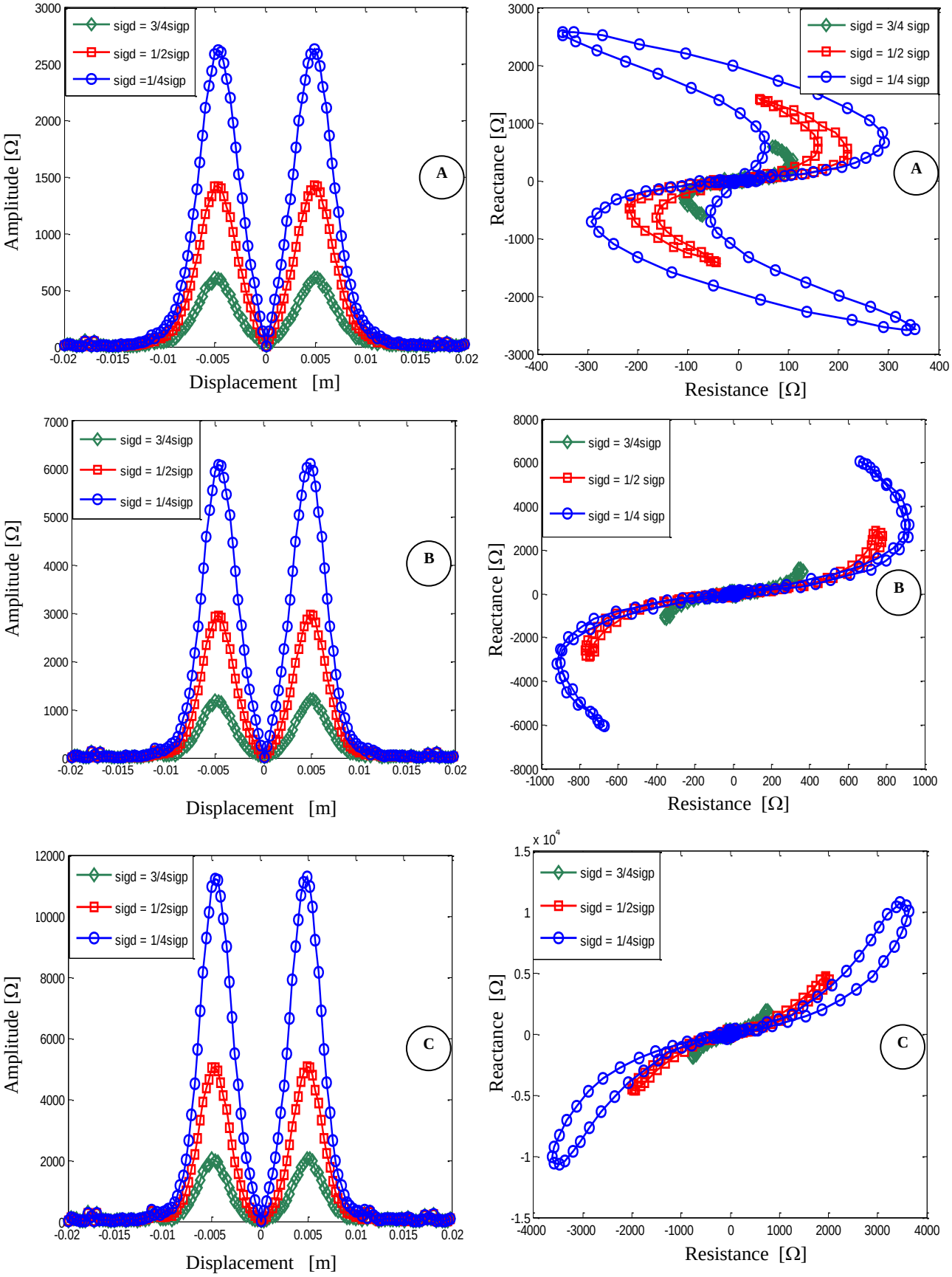

Fig. 4 Evolution of sensor impedance parameters according to defect electric conductivity.
(A): f=100kHz, (B): f=240kHz, (C): f=500kHz,

Through the results shown in Fig. (4), one can remark that the amplitude of the sensor impedance depends considerably on the defect conductivity. These results can be interpreted by the fact that as well as the difference in the conductivity between the piece and the defect is increased the sensor impedance amplitude increases. Besides, the differential impedance phase varies in anti clockwise with the increase of defect conductivity.

For better understanding the previous results at the frequency of 240 kHz, we present the evolution of the magnetic potential vector for three values of electric conductivity (A, B and C).

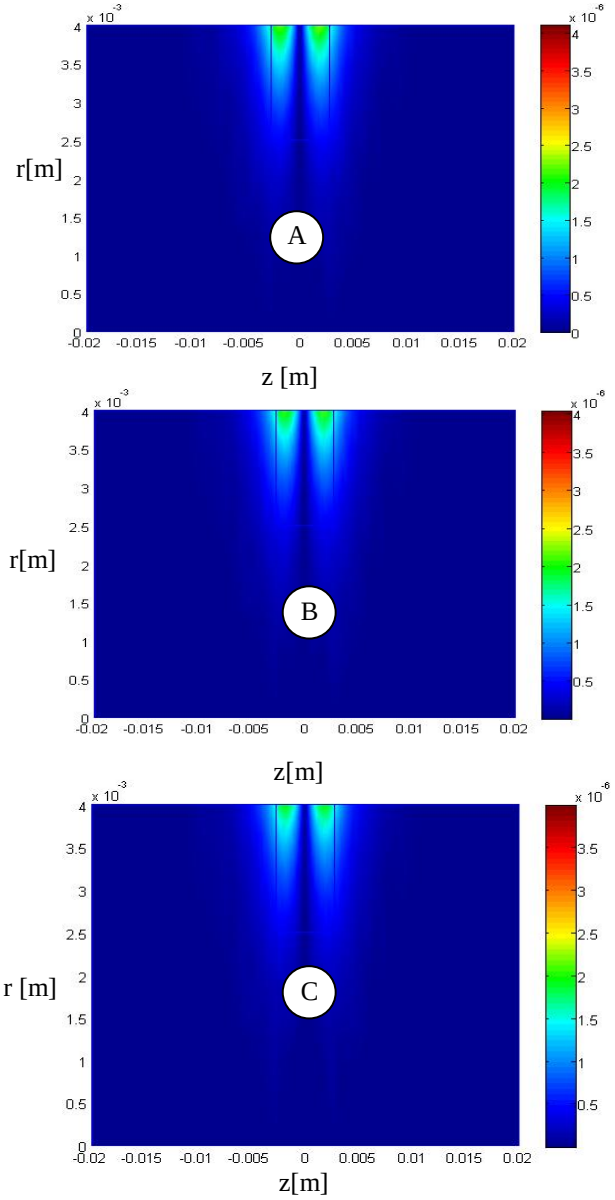

Fig. 5 Distribution of magnetic potential vector for three values of defect electric conductivity.

(A): $\sigma_d = \frac{1}{4}\sigma_p$, (B): $\sigma_d = \frac{1}{2}\sigma_p$, (C): $\sigma_d = \frac{3}{4}\sigma_p$

According to Fig. (5), one can notice that the amplitude of the magnetic potential vector is affected by the variation of the defect electric conductivity. Therefore, it necessarily leads to the modification of the sensor impedance amplitude Fig. (4). From Fig. (4), it is clear that the signal amplitude decreases 2.2 times when the defect conductivity passes from $\frac{1}{4}\sigma_p$ to $\frac{1}{2}\sigma_p$; and 5.5times when the defect conductivity passes from $\frac{1}{4}\sigma_p$ to $\frac{3}{4}\sigma_p$. These results reveal the necessity to take into account this defect physical characteristic that can be the reason of the accumulation of a layer conducting deposit in the crack.

8. Conclusion

In this article, we have studied the influence of the physical and geometrical parameters of a conductive defect on differential sensor impedance. The studied geometrical and physical parameters are the defect depth, width and electric conductivity. The defect is located in the outer rod surface on which a differential probe operates. The sensor impedance variation, caused by the presence of the defect, is calculated using the classical finite element method that we have successfully implemented in Matlab software for three different frequencies 100 kHz, 240 kHz and 500 kHz [13-14]. The obtained simulation results reveal that the depth variation generates an alteration in the sensor impedance amplitude and phase. Furthermore, the defect width variation has no influence on the amplitude and the phase, whereas the distance between the two amplitude peaks depends strongly on this parameter. Besides, the effect of the defect electric conductivity has been considered. According to the yielded simulation results, one can clearly notice that the signal amplitude decreases with 2.2 times when the defect conductivity varies from (1/4) σ_p to (1/2) σ_p; and 5.5 times when the defect conductivity varies from (1/4) σ_p to (3/4) σ_p. This study brings into evidence the necessity to take into account this defect physical characteristic so as to ensure a full and accurate defect characterization.

9. References

1. Luis S. R., João C. Gonzalezd., Telmo G. S., Pedro M. R. and Moisés P.: *Geometric optimization of a differential planar eddy currents probe for non-destructive testing*. Sensors and Actuators, Vol.197, 2013, p. 96– 105.

2. Anders Rosell and Gert Persson.:*Finite element modeling of closed cracks in eddy current testing, International Journal of Fatigue*, Elsevier, 41,2012, p. 30–38,.

3. Bouchala T., Abdelhadi B. and Benoudjit. *A.*: *Novel coupled electric field method for defect characterization in eddy current non-destructive testing Systems*, Journal of Nondestructive

Evaluation, 2013, Springer Science+ Business Media, New York, USA, Published online

4. Uwe Tröltzsch, Frank Wendler and Olfa Kanoun. :*Simplified analytical inductance model for a single turn eddy current sensor*, Elsevier, Sensors and Actuators A, Vol. 191, 2013, p.11-21.

5. Udpa L. and Lord W., *Impedance and mesh Structure considerations in the finite element analysis of eddy current NDT probe phenomena*. IEEE Transactions on Magnetics, Vol. MAG-21, No.6, 1985, p. 2268-2272.

6. Shao K. R., Youguang G. and Lavers, J. D.: *Multiresolution analysis for reconstruction of conductivity profiles in eddy current nondestructive evaluation using probe impedance data*. IEEE Transactions on Magnetics,Vol.40, 2004. 2101–2103.

7. Yu Yating and Du Pingan: *Optimization of an Eddy Current Sensor using Finite Element Method*. Proceedings of the (2007) IEEE International Conference on Mechatronics and Automation, August 5 - 8, 2007, Harbin, China, p. 3775-3800.

8. Yating Y. Pingan D. and Lichuan X.: *Coil impedance calculation of an eddy current sensor by the finite element method. Russian Journal of Nondestructive Testing*, Vol. 44, No. 4, 2008 p. 296–302.

9. Veeraraghavan Sundararaghavan, Krishnan Balasubramaniam, Nimmagadda Ramesh Babub, Nataraja Rajesh.: *A Multi-Frequency Eddy Current Inversion method for characterizing conductivity gradients on water Jet peened components*, NDT&E International, Vol. 38, 2005, p.541–547.

10. Ida N. and Lord W., *A finite element model for three-dimensional eddy current NDT phenomena*, IEEE Transactions on Magnetics., Vol. MAG-21, No. 6, 1985, p. 2635.

11. Javier G.-M., Jaime G.-G. and Ernesto, V.-S.,: *Non-destructive techniques based on eddy current testing*. Sens. J., 2011, p.2525–2565.

12. Maouche B., Rezak A. and Feliachi M.: *Semi analytical calculation of the impedance of differential sensor for eddy current non destructive testing*. In: NDT & E International, Elsevier, Amsterdam, Vol. 42, 2009, p.573–580.

13. Rachek M., Cherif S. and Kadi H. :*Strong Coupled Formulation of the Magnetic Vector Potential and Total Current Density for Eddy Current Testing with Skin and Proximity Effects*. The International Conference on Electronics & Oil from Theory to Application. March 05-06, 2013, Ouargla, Algeria.

14. Bouchala T., Abdelhadi B. and Benoudjit A.: *Fast analytical modeling of eddy current nondestructive testing of magnetic material*. Journal of Nondestructive Evaluation, Springer Science + Business Media , New York, USA, Vol. 32, 2013, Issue 3, p.294-299.